CMI

www.nature.com/cmi

ARTICLE

Check for updates

Enhanced CD19 activity in B cells contributes to immunodeficiency in mice deficient in the ICF syndrome gene *Zbtb24*

Zhengzhou Ying[1,3], Swanand Hardikar[1], Joshua B. Plummer[1], Tewfik Hamidi[1], Bin Liu[1,2], Yueping Chen[1], Jianjun Shen[1,2], Yunxiang Mu[1], Kevin M. McBride[1,2]✉ and Taiping Chen[1,2]✉

Immunodeficiency, centromeric instability, and facial anomalies (ICF) syndrome is a rare autosomal recessive disorder characterized by DNA hypomethylation and antibody deficiency. It is caused by mutations in *DNMT3B*, *ZBTB24*, *CDCA7*, or *HELLS*. While progress has been made in elucidating the roles of these genes in regulating DNA methylation, little is known about the pathogenesis of the life-threatening hypogammaglobulinemia phenotype. Here, we show that mice deficient in *Zbtb24* in the hematopoietic lineage recapitulate the major clinical features of patients with ICF syndrome. Specifically, Vav-Cre-mediated ablation of *Zbtb24* does not affect lymphocyte development but results in reduced plasma cells and low levels of IgM, IgG1, and IgA. *Zbtb24*-deficient mice are hyper and hypo-responsive to T-dependent and T-independent type 2 antigens, respectively, and marginal zone B-cell activation is impaired. Mechanistically, *Zbtb24*-deficient B cells show severe loss of DNA methylation in the promoter region of *Il5ra* (interleukin-5 receptor subunit alpha), and *Il5ra* derepression leads to elevated CD19 phosphorylation. Heterozygous disruption of *Cd19* can revert the hypogammaglobulinemia phenotype of *Zbtb24*-deficient mice. Our results suggest the potential role of enhanced CD19 activity in immunodeficiency in ICF syndrome.

Keywords: ICF syndrome; ZBTB24; CD19; IL-5Ra; hypogammaglobulinemia

Cellular & Molecular Immunology (2023) 20:1487–1498; https://doi.org/10.1038/s41423-023-01106-w

INTRODUCTION

Immunodeficiency, centromeric instability and facial anomalies (ICF) syndrome is a rare autosomal recessive disorder characterized by antibody deficiency, facial dysmorphism, developmental delay, and intellectual disability [1, 2]. A cytogenetic feature of ICF syndrome is chromosomal rearrangements due to DNA hypomethylation of satellite repeats at (peri)centromeric heterochromatin [1, 3–6]. ICF syndrome is caused by mutations in one of four known genes—*DNMT3B* (ICF1), *ZBTB24* (ICF2), *CDCA7* (ICF3), and *HELLS* (ICF4)—with ICF1 (~50%) and ICF2 (~30%) accounting for most cases [7–13]. Recent evidence suggests that the four gene products are components of a molecular pathway that regulates DNA methylation. Specifically, ZBTB24, a member of the zinc-finger (ZF)- and BTB domain-containing (ZBTB) family of transcriptional regulators, induces *CDCA7* expression, and CDCA7 recruits HELLS, a DNA helicase involved in chromatin remodeling, to specific genomic regions to facilitate DNA methylation by the DNA methylation machinery, including DNMT3B [14–19].

Patients with ICF syndrome suffer from recurrent and often fatal infections in early childhood due to hypogammaglobulinemia or agammaglobulinemia. While they usually have normal counts of T and B lymphocytes, phenotypic analysis revealed the presence of only naïve B cells and the absence of memory B cells and plasma cells, suggesting impaired B-cell activation and/or terminal differentiation [20]. However, the cellular and molecular defects underlying antibody deficiency in ICF syndrome remain poorly understood.

B-cell survival and differentiation are tightly controlled by signaling from the B-cell receptor (BCR), a transmembrane complex composed of a membrane-bound immunoglobulin (Ig) and the signal transduction components Igα/Igβ (CD79a/CD79b). The BCR transmits constitutive, tonic signals necessary for survival in the absence of antigen binding and activation signals following antigen engagement [21]. For mature B cells in the periphery, BCR engagement activates signaling pathways that induce proliferation and transcriptional programs for differentiation into germinal centers (GCs), memory and plasma cells [22]. However, during early B-cell development, BCR activation plays a key role in central tolerance. BCR engagement in bone marrow (BM) immature cells facilitates the elimination of self-reactive BCRs [23]. Thus, BCR

[1]Department of Epigenetics and Molecular Carcinogenesis, The University of Texas MD Anderson Cancer Center, Houston, TX 77030, USA. [2]Program in Genetics and Epigenetics, The University of Texas MD Anderson Cancer Center UTHealth Graduate School of Biomedical Sciences, Houston, TX 77030, USA. [3]Present address: The Ministry of Education Key Laboratory of Laboratory Medical Diagnostics, College of Laboratory Medicine, Chongqing Medical University, Chongqing 400016, China. ✉email: KMcBride@mdanderson.org; TChen2@mdanderson.org

Received: 19 April 2023 Accepted: 31 October 2023
Published online: 22 November 2023

activation controls B-cell fate in a context- and developmental stage-dependent manner.

CD19, a transmembrane protein expressed throughout B-cell development, modulates BCR signaling. CD19-deficient (*Cd19*$^{-/-}$) mice develop B cells but have reduced peripheral populations and deficient GC, B1, and marginal zone (MZ) compartments [24]. B cells without CD19 are hyporesponsive to BCR engagement with reduced phosphorylation of signaling factors, reduced proliferation, and loss of terminal differentiation [25]. CD19 overexpression results in the opposite phenotype, as B cells from human CD19-transgenic (hCD19TG) mice display enhanced BCR signaling and an elevated antibody response. hCD19TG mice also have reduced levels of naïve cells leaving the BM, presumably due to overactive negative selection [26]. Further characterization of *Cd19*$^{-/-}$ and hCD19TG mice revealed that CD19 enhances humoral immune responses to T-dependent (TD) antigens but inhibits humoral immune responses to T-independent type 2 (TI-2) antigens [27]. Thus, CD19 has been proposed to function as a critical rheostat that amplifies BCR signaling and lowers thresholds for activation [28]. While the relationship between BCR and CD19 signaling is well established, the full catalog of factors that influence this signaling axis remains to be defined.

In this study, we show that conditional ablation of *Zbtb24* in the hematopoietic lineage in mice results in a phenotype that mimics major clinical manifestations of ICF syndrome, including normal T- and B-cell development, reduced plasma cells, and hypogammaglobulinemia. We provide evidence that Zbtb24 is a negative regulator of CD19 activity, as *Zbtb24*-deficient B cells display elevated CD19 phosphorylation, which contributes to hypogammaglobulinemia. Mechanistically, *Il5ra* [encoding the IL-5-binding subunit (α chain) of the IL-5 receptor (IL-5Rα)], which is normally repressed in most resting B cells, is derepressed in *Zbtb24*-deficient B cells due to severe loss of promoter methylation, resulting in enhanced CD19 phosphorylation.

MATERIALS AND METHODS

Mice

All animal experiments were performed under protocols approved by the Institutional Animal Care and Use Committee at The University of Texas MD Anderson Cancer Center. The *Zbtb24* conditional allele (*Zbtb24*^{2lox}) was generated by gene targeting using homologous recombination. Briefly, mouse embryonic stem cells (mESCs) were transfected with the targeting vector (Fig. S1A) via electroporation and selected with Geneticin (G418). Correctly targeted mESC clones (*Zbtb24*$^{3lox/+}$), identified by Southern blotting (Fig. S1B), were injected into blastocysts to obtain chimeric mice, which were then crossed with wild-type (WT) mice to obtain F1 mice with germline transmission of the *Zbtb24*^{3lox} allele. Germline deletion of the *IRES-βGeo* selection cassette (flanked by *FRT* sites, Fig. S1A), resulting in the *Zbtb24*^{2lox} allele (Fig. S1C), was achieved by crossing *Zbtb24*$^{3lox/+}$ mice with FLPeR mice, which constitutively express the FLPe recombinase [29]. *Zbtb24*$^{2lox/+}$ mice, which were initially C57BL/6-129 hybrids, were back-crossed with C57BL/6 mice for six generations. Deletion of the floxed region, resulting in the null allele (*Zbtb24*$^{-}$) (Fig. S1D), in the germline and hematopoietic, T-cell, and B-cell lineages was achieved by crossing mice carrying the *Zbtb24*^{2lox} allele with Zp3-Cre [30], Vav-Cre [31], Lck-Cre [32], and CD19-Cre [33] mice, respectively. All primers used in the study, including those for genotyping and for generating the *Zbtb24* gene targeting vector, are listed in Table S1.

Immunization

For TD antigen immunization, 8- to 10-week-old mice were intraperitoneally (i.p.) injected with 100 μg of nitrophenyl-conjugated keyhole limpet hemocyanin (NP-KLH) (Biosearch Technologies) in saline supplemented with 50% (vol/vol) alum (Thermo Fisher Scientific) and, if applicable, were boosted 60 days later with NP-KLH in saline. Sera were collected from the mice before immunization (day 0); at days 14, 28, and 56 after the first exposure; and, if applicable, on day 14 after the boost. For TI antigen immunization, 8- to 10-week-old mice were i.p. injected with 100 μg of NP-lipopolysaccharide (LPS), NP-Ficoll, or NP-dextran in saline. Sera were collected from the mice on days 0, 6, and 14. The titers of NP-specific antibody isotypes in sera were measured by ELISA using plates coated with NP(7)-BSA or NP(20)-BSA (Biosearch Technologies) as described previously [34].

ELISA

Serum concentrations of total IgG1, IgG2a, IgG2b, IgG3, IgM, and IgA were determined by using the Clonotyping System-HRP (Southern Biotech) with the Mouse Ig Isotype Panel (Southern Biotech) as a positive reference standard according to the manufacturer's instructions. For the determination of NP-specific antibodies, ELISAs were performed as described previously [34].

Serum IL-5 cytometric bead assay

Serum samples from WT and VAV-CKO mice were diluted as described in the BD CBA Mouse/Rat Soluble Protein Master Buffer Kit (BD Biosciences 558266) and tested using the BD CBA Mouse IL-5 Flex Set (BD Biosciences 558302). Bead populations were analyzed using a BD LSRFortessa instrument, and MFI values were calculated using FlowJo software (BD Biosciences).

Flow cytometry

The following antibodies/reagents (purchased from BD Bioscience) were used for staining: B220–APC-H7, CD3-PE, IgM-PE-CY7, IgD-PE, CD43-PE, CD11b-PERCP-CY5.5, CD4-APC-H7, CD8-PE-CY7, CD23- FITC, CD21/35-APC, CD19–FITC, CD19-Alexa-R600, CD62L-FITC, CD44-PE, CD138-PE, IgG1-APC, GL7-FITC, CD95-PE, and propidium iodide. The CellTrace Violet (CTV) Cell Proliferation Kit was purchased from Thermo Fisher Scientific. Single-cell BM or spleen cell suspensions were prepared and stained [34] for analysis and sorting using either a Fortessa flow cytometer (BD Bioscience) or FACSFusion flow cytometer (BD Bioscience). Further analysis was conducted with FlowJo software (v9) for gating and analysis.

Immunofluorescence

Mice were sacrificed, and their spleens were quickly removed and embedded in Tissue-Tek O.C.T. COMPOUND (ProSciTech) and snap-frozen in liquid nitrogen. Cryosections (20 μm) were air-dried for 30 min and then fixed in acetone for 10 min. The sections were air-dried for another 30 min and rehydrated for 10 min in PBS. After blocking with antibody dilution buffer [2% goat serum (Sigma–Aldrich) and 1% BSA in PBS] for 30 min, sections were incubated with B220-, CD4- or PNA-FITC (Sigma–Aldrich) overnight at 4 °C. After being washed, sections were permeabilized with 0.1% Triton X-100 (Sigma–Aldrich) in PBS for 5 min. Following the final washing, sections were mounted with Mounting Reagent with DAPI (Life Technologies). Confocal microscopy was performed with a Zeiss LSM880 microscope.

RNA sequencing (RNA-Seq)

Splenic MZ and follicular (FO) B cells were sorted using mouse MZ and FO B-Cell Isolation Kit with LS columns (Miltenyi) according to the manufacturer's instructions. Total RNA from the sorted B cells was isolated with an RNeasy Mini Kit (Qiagen). The libraries for RNA-Seq were sequenced using a 2 × 75-base paired-end protocol on an Illumina HiSeq 3000 instrument. A total of 60–70 million pairs of reads were generated per sample. The raw RNA-Seq readouts were mapped to the mouse assembly reference genome (GRCm38) using TopHat2 and Bowtie2 [35, 36], open-source software tools that align RNA-Seq reads to a reference genome. The raw read counts were generated by using HTSeq-count from the HTSeq package (version 0.6.1p1) [37]. The overall mapping rates by reads were 92-96%. Differential gene expression analysis was performed with DESeq2 (a R/Bioconductor package) [38], using adjusted p value < 0.05 as the significance cutoff. The RNA-Seq data are available in the Gene Expression Omnibus database with accession number GSE184699.

RT-qPCR

Total RNA was isolated with TRIzol (Invitrogen) and treated with RNase-free DNase I (Thermo Fisher Scientific). Reverse transcription (RT) was performed using a ProtoScript First Strand cDNA Synthesis kit (New England Biolabs) to generate cDNAs. RT-qPCR was performed using iTaq Universal SYBR Green PCR Master Mix (Bio-Rad) on an ABI 7900 Real-Time PCR system (Thermo Fisher Scientific). The primer sequences are listed in Table S1.

Western blotting

Cell lysates were prepared in lysis buffer (50 mM Tris-HCl, pH 7.5, 150 mM NaCl, 0.2 mM EDTA, and 0.1% Nonidet P-40) supplemented with protease and phosphatase inhibitor cocktail (Thermo Fisher Scientific). A total of 50–100 μg of protein was resolved by SDS–PAGE and transferred to a polyvinylidene difluoride membrane. The following primary antibodies were used: Zbtb24 (MBL, PM085), CD19 [Cell Signaling Technology (CST), 3574], phospho-CD19 (Tyr531) (CST, 3571), phospho-Akt (CST, 9271), phospho-PLCγ (CST, 50535), phospho-CD79a (CST, 5173), β-actin (Sigma–Aldrich, A5441), and HA tag (CST, 3724). Primary antibodies were detected with HRP-conjugated goat anti-rabbit (Pierce), goat anti-mouse (Pierce), or goat anti-guinea pig (Southern Biotech) secondary antibodies, followed by enhanced chemiluminescence (ECL) with a detection kit (GE Healthcare).

B-cell culture, activation, and proliferation

FO and MZ B cells sorted from mice and the CH12F3 cell line were maintained in RPMI 1640 medium supplemented with 10% FBS and 0.05 mM 2-mercaptoethanol. To trace cell proliferation, FO and MZ B cells were labeled with CTV (Thermo Fisher Scientific), treated with either 10 μg/ml $F(ab')_2$ fragment goat anti-mouse IgM (Jackson ImmunoResearch) or LPS (Sigma–Aldrich) for 72 h and analyzed by flow cytometry. For cell activation, naïve B cells or CH12F3 cells were treated with 10 μg/ml $F(ab')_2$ fragment goat anti-mouse IgM or 10 ug/ml mIL-5 (R&D Systems) for 5 or 10 min and then collected for Western blotting or RNA extraction.

Protein overexpression, mRNA knockdown (KD), and CRISPR gene editing in CH12F3 cells

Lentiviral supernatants were produced by cotransfection of the packaging vectors *pMD2.G* (Addgene, #12259) and *psPAX2* (Addgene, #12260) and *pCDH-EF1-FHC* vector (Addgene, #64874) expressing HA-Crisp3 or HA-IL-5Rα, *pLKO.1 puro* vector (Addgene, #8453) expressing control (shControl) or *Il5ra* shRNAs (shIl5ra-1 to shIl5ra-4), or *pL-CRISPR.EFS.GFP* vector (Addgene, #57818) expressing the *Zbtb24* sgRNAs and Cas9 into 293 T cells and collected 48 h after transfection. For infection, CH12F3 cells (5×10^5 cells/ml) were cultured in 2 ml of medium and 200 μl of viral supernatants supplemented with polybrene (0.5 μg/ml) for 24 h. For protein overexpression and shRNA-mediated KD, the cells were selected with puromycin (1 μg/ml) for 1 week, and viable cells were sorted by FACS to derive KD cell pools. For gene editing with CRISPR/Cas9 technology, GFP^+ cells were sorted 24 h after infection (without selection), and single cells were seeded into a 96-well plate to derive pure clones.

DNA methylation analysis by bisulfite sequencing

Bisulfite sequencing analysis of CpG methylation was performed as described previously [39, 40]. A 148-bp region in the *Il5ra* promoter (from −1489 to −1342 upstream of the transcription start site), containing seven CpG sites, was analyzed. The primers used are listed in Table S1.

Statistical analysis

The results were analyzed by using GraphPad Prism and are expressed as the median with interquartile range or means ± SDs. The statistical significance was analyzed by *t* test with Mann Whitey test, one-way or two-way ANOVA multiple comparisons vs. WT or control, as indicated in the figure legends.

RESULTS

Mice deficient in *Zbtb24* in hematopoietic cells recapitulate the antibody deficiency phenotype of ICF syndrome

To investigate the biological functions of Zbtb24, we generated a *Zbtb24* conditional allele ($Zbtb24^{2lox}$) in mice, which contains two *loxP* sites flanking a 1.3-kb region including exon 2. Cre-mediated deletion of the floxed region removes the N-terminal 316 amino acids that include the BTB domain, AT-hook, and part of the ZF domain, resulting in a null allele ($Zbtb24^{-}$) (Fig. S1A). Genotypes were determined by Southern blotting and PCR (Fig. S1B–D). $Zbtb24^{2lox/2lox}$, $Zbtb24^{2lox/-}$ and $Zbtb24^{+/-}$ mice were all grossly normal and fertile. However, intercrosses between $Zbtb24^{+/-}$ or $Zbtb24^{2lox/-}$ mice produced no viable pups with homozygous deletion ($Zbtb24^{-/-}$). Timed mating revealed that $Zbtb24^{-/-}$ embryos were arrested before 8.5 days post coitum (Fig. S1E), in agreement with a previous report [14]. Thus, *Zbtb24* is essential for embryonic development in mice, although ICF2 patients—many carrying homozygous or compound heterozygous null mutations in *ZBTB24* [10–12, 41]—are viable.

To assess the role of Zbtb24 in immune cells, we conditionally deleted *Zbtb24* in the hematopoietic lineage using Vav-Cre [31]. PCR genotyping and Western blotting confirmed efficient deletion of *Zbtb24* in B220 + B cells and CD3 + T cells but not in tail samples (Fig. 1A, B). $VavCre{:}Zbtb24^{2lox/2lox}$ (VAV-CKO) mice grew normally, were fertile, and appeared indistinguishable from $VavCre{:}Zbtb24^{2lox/+}$ (control) and WT mice. As Vav-Cre is also expressed in endothelial cells [31], our results suggest that in VAV-CKO mice, defects in endothelial cells, if any, would be minimal. However, further work needs to be done to determine *Zbtb24* expression in endothelial cells and its deletion efficiency in endothelial cells in VAV-CKO mice.

A major clinical feature of ICF syndrome is hypogammaglobulinemia [42]. We measured the basal serum Ig levels in VAV-CKO mice. Lower levels of IgG1 and IgM were detected in *Zbtb24*-deficient mice as early as 3 weeks of age (Fig. 1C). At the adult stage (8–10 weeks of age), VAV-CKO mice, relative to control mice, showed significantly lower levels of IgG1, IgM, and IgA, slightly lower levels of IgG2a, and comparable levels of IgG2b and IgG3 (Fig. 1D). Older (6-month-old) VAV-CKO mice also showed significant decreases in IgG1, IgM, and IgA (Fig. 1E), suggesting the persistence of the hypogammaglobulinemia phenotype. Indeed, with increasing Ig levels over time, the differences between control and *Zbtb24*-deficient mice seemed to become more evident (Fig. 1C–E). Control and VAV-CKO mice showed no differences in cytokine secretion by helper T cells, including IFNγ, IL-4, IL-2, and IL-17 (Fig. 1F–H), suggesting that hypogammaglobulinemia induced by *Zbtb24* deficiency was caused by B-cell-intrinsic defects. Consistent with this notion, Lck-Cre-mediated *Zbtb24* deletion in the T-cell lineage had no effects on basal serum Ig levels, T-cell subtypes in the spleen, or the humoral immune response to the TD antigen NP-KLH (Fig. S2A–C).

VAV-CKO mice show no defects in lymphocyte development but have decreased plasma cells

To explore the cellular defects underlying hypogammaglobulinemia in VAV-CKO mice, we examined lymphocyte subtypes. Flow cytometry showed that *Zbtb24*-deficient mice had normal percentages of B lineage (B220+), T lineage (CD3+), and myeloid lineage (CD11b+) cells in BM (Fig. S3A, B) and normal total cell numbers in BM and spleen (Fig. S3C, D). Analysis of pro-B, pre-B, immature and mature B cells in BM indicated that B-cell development progressed normally in the absence of Zbtb24 (Figs. 2A, S3E). Early subtypes of T-cell development in the thymus were also normal in VAV-CKO mice (Fig. S3F, G). In addition, *Zbtb24* deficiency had no effect on the subpopulations of naïve B cells in the spleen, including FO, MZ, and transitional B cells (Fig. 2B, Fig. S3H). Similarly, the frequencies of naïve, effector, and memory T-cell subtypes in the spleen showed no differences between VAV-CKO and control littermates (Fig. 2C, Fig. S3I). However, there were significant decreases in the frequencies and numbers of plasma cells in the BM and spleen of *Zbtb24*-deficient mice (Fig. 2D–G). These results, which are consistent with the observation that ICF patients have normal B- and T-cell counts [43, 44], suggest that Zbtb24 is not needed for lymphocyte development but plays a role in B-cell activation and/or terminal differentiation.

VAV-CKO mice show divergent humoral immune responses to T-dependent and T-independent antigens

To assess the impact of *Zbtb24* deficiency on lymphocyte functions, we immunized mice with TD and TI antigens. Flow cytometry revealed that unimmunized (day 0) control and VAV-CKO mice had similarly low percentages and numbers of GC

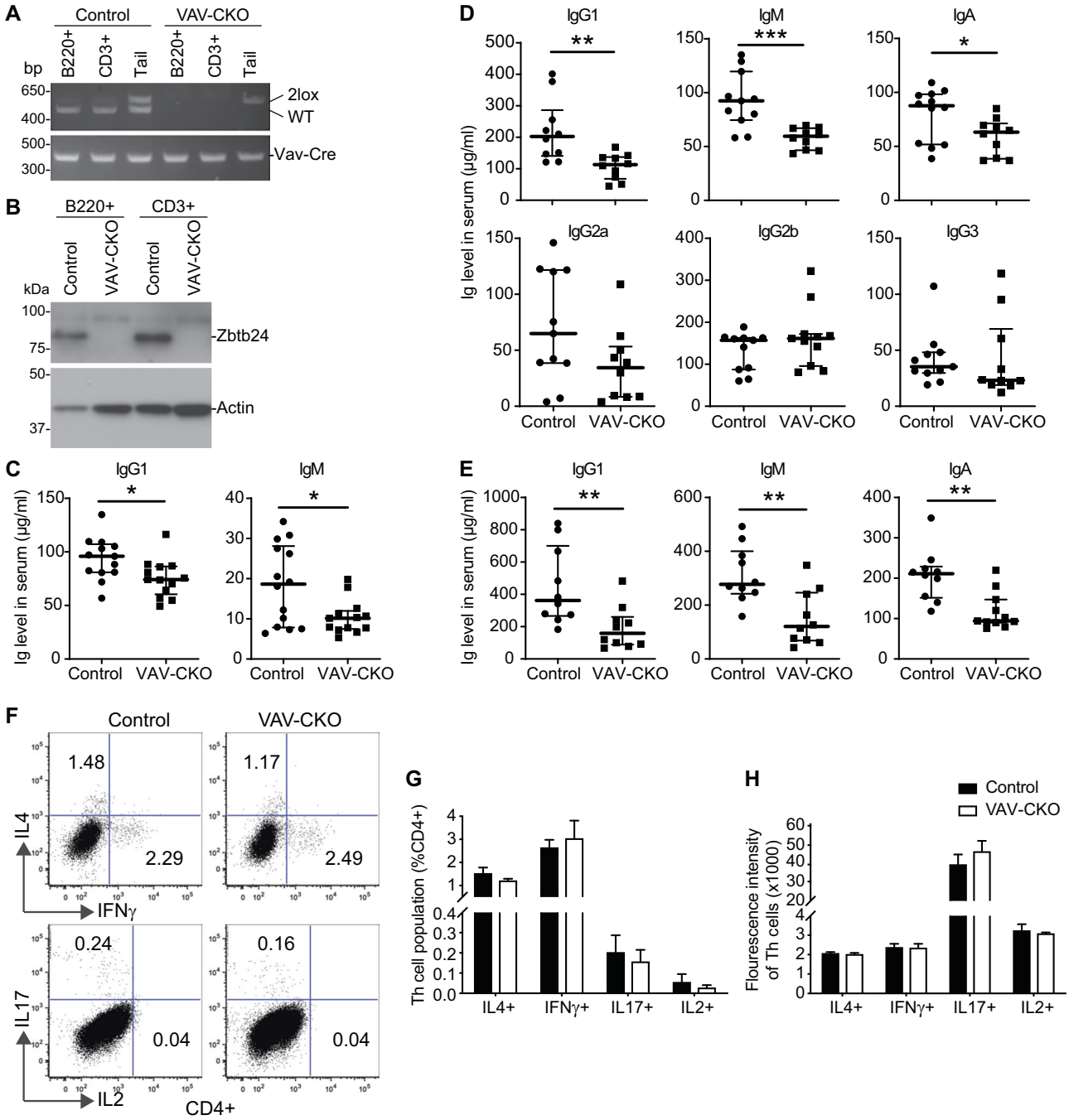

Fig. 1 VAV-Cre-mediated *Zbtb24* ablation results in hypogammaglobulinemia in mice. **A** PCR genotyping of sorted B220 + B cells and CD3 + T cells and tail DNA from Control (*VavCre:Zbtb24*$^{2lox/+}$) and VAV-CKO (*VavCre:Zbtb24*$^{2lox/2lox}$) mice. **B** Western blot showing Zbtb24 depletion in sorted B220 + B cells and CD3 + T cells from VAV-CKO mice. **C–E** ELISA analysis of sera from control and VAV-CKO mice showing basal levels of IgG1 and IgM at 3 weeks of age (**C**); IgG1, IgM, IgA, IgG2a, IgG2b, and IgG3 at 8–10 weeks of age (**D**); and IgG1, IgM, and IgA at 6 months of age (**E**). **F–H** Analysis of IL4-, IFNγ-, IL17-, and IL2-producing CD4+ cells in spleens from control and VAV-CKO mice. Representative flow cytometry data (**F**), percentages of Th subpopulations in CD4+ cells (**G**), and fluorescence intensity of Th cells (**H**) are shown. Data (median with interquartile range) from 10 to 14 (**C–E**) and 8 (**G**, **H**) mice are presented. Statistical analysis was performed using t test with the Mann–Whitney test. *$P < 0.05$; **$P < 0.01$; ***$P < 0.001$

(GL7+Fas+) B cells in their spleens. Fourteen days after immunization with NP-KLH, a TD antigen, all mice had significantly higher numbers of GC B cells in their spleens, but the increases were consistently greater in VAV-CKO mice (>10-fold) than in control mice (~5-fold) (Fig. 3A, B, Fig. S4A). Immunofluorescence staining of spleen sections with peanut agglutinin (PNA) also showed increases in the numbers and sizes of GCs in *Zbtb24*-deficient mice (Fig. S4B, C). As measured by ELISA in sera collected 14, 28, and 56 days after NP-KLH injection, steady increases in low-affinity (anti-NP20) and high-affinity (anti-NP7) IgG1 against NP and transient increases in low- and high-affinity IgM against NP were observed in both control and VAV-CKO mice, with significantly higher titers in *Zbtb24*-deficient mice (Fig. 3C, D). IgA and IgG2a were undetectable on day 14 after immunization, and IgG2b and IgG3 responses were comparable in control and VAV-CKO mice at all time points examined (Fig. S4D). In sera

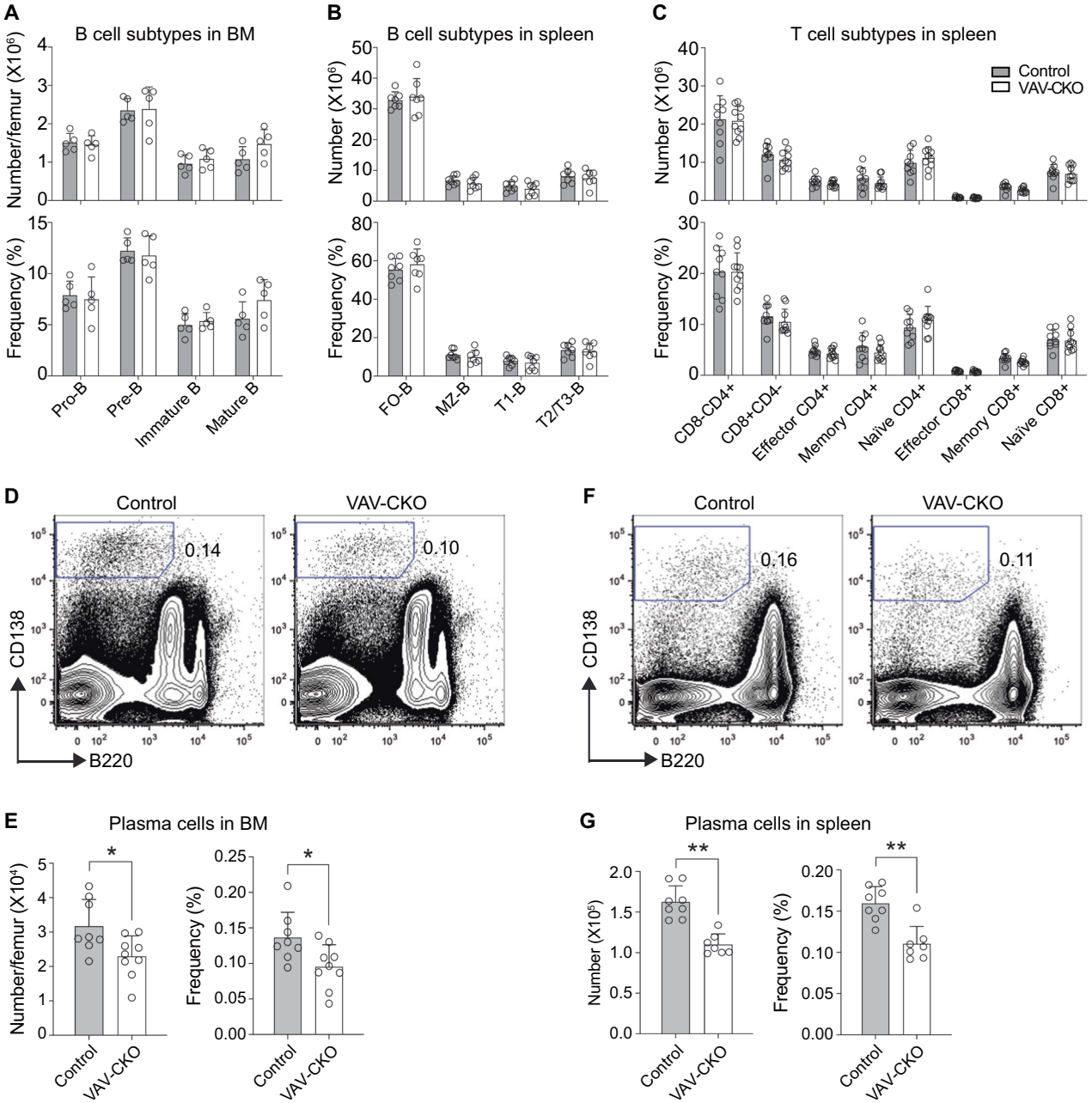

Fig. 2 *Zbtb24* deficiency has no effect on B- and T-cell development but leads to decreased plasma cells. **A**–**C** Numbers (top) and frequencies (bottom) of B cells at various maturation stages [pro-B (B220 + CD43+), pre-B (B220 + CD43-IgM-IgD-), immature (B220 + CD43-IgM+IgD-), and mature (B220 + CD43-IgM+IgD+) B cells] in BM (**A**), various B-cell subtypes [FO (B220 + CD93-CD23 + CD21/35lo), MZ (B220 + CD93-CD23-CD21/35hi), T1 (B220 + CD93 + CD23-), and T2/T3 (B220 + CD93 + CD23+) B cells] in spleen (**B**) and various T-cell subtypes [helper (CD8-CD4+), cytotoxic (CD8 + CD4-), effector helper (CD4 + CD8-CD44 + CD62L-), memory helper (CD4 + CD8-CD44 + CD62L+), naïve helper (CD4 + CD8-CD44-CD62L+), effector cytotoxic (CD4-CD8 + CD44 + CD62L-), memory cytotoxic (CD4-CD8 + CD44 + CD62L+), and naïve cytotoxic (CD4-CD8 + CD44-CD62L+) T cells] in spleen (**C**) from Control and VAV-CKO mice. **D**–**G** Flow cytometry analysis of plasma cells (CD11b-CD3-B220lo/CD138hi) in BM (**D**, **E**) and spleen (**F**, **G**) from Control and VAV-CKO mice. Representative flow cytometry data (**D**, **F**) and absolute numbers (left) and frequencies (right) of plasma cells (**E**, **G**) are shown. Presented in (**A**, **B**, **C**, **E**, **G**) are data (mean ± SD) from 5 to 9 mice. Statistical analysis was performed using t test with the Mann–Whitney test. *$P < 0.05$; **$P < 0.01$

collected 14 days after the secondary immunization (administered 60 days after the primary immunization), significantly higher titers of low-affinity and comparable levels of high-affinity anti-NP-specific IgG1 and IgM were detected in VAV-CKO mice than in control littermates (Fig. 3E, F). Based on the ratios of high-affinity to low-affinity antibodies (Fig. 3G, H), VAV-CKO mice tended to produce low-affinity IgG1 and IgM. Of note, previous work reported that mice deficient in *Dnmt3b* (another ICF-related gene) and its paralog *Dnmt3a* in B cells also show normal B-cell development but exhibit enhanced TD responses upon immunization [45].

While hyperresponsive to TD antigens, *Zbtb24*-deficient mice had lower natural antibodies (Fig. 1C–E), suggesting that immune responses to T-independent antigens may also be perturbed by loss of Zbtb24. There are two categories of TI antigens: TI-1 antigens have the ability to directly activate B cells, and TI-2

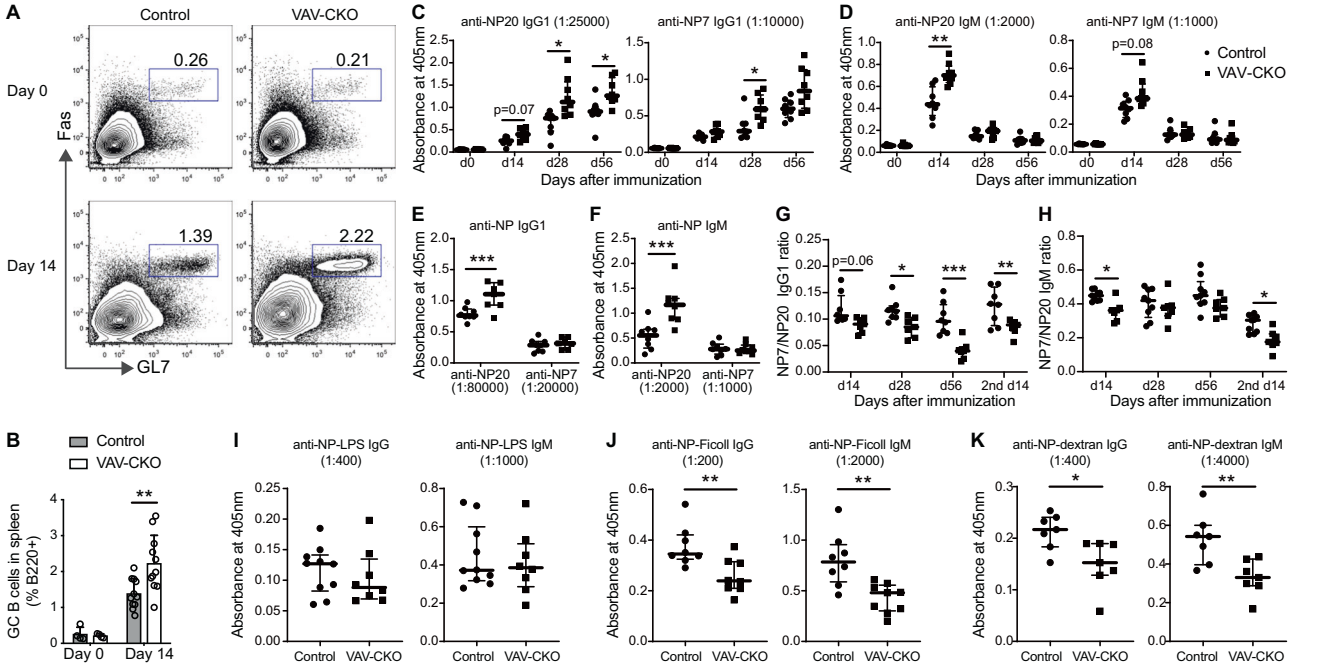

Fig. 3 *Zbtb24*-deficient mice show different humoral immune responses to T-dependent and T-independent antigens. **A, B** Flow cytometry analysis of germinal center (GC) B cells (B220 + GL7+Fas+) before (day 0) and 14 days after immunization with NP-KLH in spleens from Control and VAV-CKO mice. Representative flow cytometry data (**A**) and frequencies of GC B cells (percentages in B220+ cells) in the spleen (**B**) are shown. **C**–**F** Relatively low-affinity (NP20) and high-affinity (NP7) anti-NP-specific IgG1 (**C**, **E**) and IgM (**D**, **F**) antibody absorbance by ELISA in sera from Control and VAV-CKO mice on day 0, day 14, day 28, and day 56 after the first injection with NP-KLH (**C**, **D**) and on day 14 after the second injection with NP-KLH (**E**, **F**). **G, H** Ratio of high-affinity to low-affinity IgG1 (**G**) and IgM (**H**) in Control and VAV-CKO mice on day 0, day 14, day 28, and day 56 after the first injection with NP-KLH and on day 14 after the second injection with NP-KLH. **I**–**K** Anti-NP-specific IgG and IgM antibody absorbance by ELISA in sera from control and VAV-CKO mice on day 6 after immunization with NP-LPS (**I**), NP-Ficoll (**J**), or NP-dextran (**K**). Data (median with interquartile range) from 8 to 10 mice are presented in (**C**–**K**). Statistical analysis was performed using two-way ANOVA (**C**–**H**) or t test with Mann Whitey test (**I**–**K**). *$P < 0.05$; **$P < 0.01$; ***$P < 0.001$

antigens are typically repeating polymers and cause simultaneous crosslinking of BCRs on B lymphocytes. After immunization with NP-LPS, a TI-1 antigen, control and VAV-CKO mice had similar titers of IgG and IgM against NP in their sera (Fig. 3I). However, after immunization with NP-Ficoll or NP-dextran, both of which are TI-2 antigens, VAV-CKO mice mounted significantly lower anti-NP-specific IgG and IgM responses than control littermates (Fig. 3J, K).

In summary, our results show that *Zbtb24* deficiency results in enhanced and diminished humoral immune responses to TD and TI-2 antigens, respectively.

Zbtb24-deficient marginal zone B cells are defective in proliferation in response to stimulation with anti-IgM

To gain insights into the intrinsic function of Zbtb24 in B cells, we tested the ability of B cells to be activated in the absence of T-cell help. FO and MZ B cells sorted from control and VAV-CKO mice were stained with CTV reagent, then stimulated with LPS or soluble F(ab')2 fragment of anti-IgM (referred to as anti-IgM hereafter), an analog of TI-2 antigen, for 72 h. Then, they were analyzed with flow cytometry to monitor cell proliferation by dye dilution. After stimulation with LPS, both FO and MZ B cells from VAV-CKO mice were activated and proliferated normally (Fig. 4A, B). After stimulation with anti-IgM, whereas the vast majority of FO B cells from VAV-CKO mice underwent proliferation, similar to those from control mice, significantly smaller proportions of *Zbtb24*-deficient MZ B cells underwent proliferation when compared to their control counterparts (Fig. 4C, D).

Enhanced CD19 activity contributes to hypogammaglobulinemia in VAV-CKO mice

Our results suggested that antibody deficiency in VAV-CKO mice was a B-cell-intrinsic phenotype (Figs. 1 and 4, Fig. S2). To further confirm this, we deleted *Zbtb24* in the B-cell lineage using CD19-Cre [33]. To our surprise, *Cd19Cre:Zbtb24*$^{2lox/2lox}$ (CD19-CKO) mice had normal levels of serum IgG1, IgM, and IgA (Fig. 5A), although Zbtb24 depletion was robust in B cells (Fig. S5A). These mice also responded normally to immunization with NP-KLH, as judged by the frequencies of total GC B cells and anti-NP-specific IgG1 and IgM GCs and memory B cells in the spleen (Fig. S5B–D). Given that one copy of *Cd19* is disrupted in CD19-Cre knock-in (KI) mice [33], it is possible that different levels of CD19 expression contribute to the phenotypic differences between CD19-CKO and VAV-CKO mice. Indeed, the divergent humoral immune responses of VAV-CKO mice to different antigens—i.e., hyperresponsive to TD and hyporesponsive to TI-2 antigens (Fig. 3)—were similar to the phenotype of hCD19TG mice and opposite to that of *Cd19*$^{-/-}$ mice [27]. We therefore asked whether *Cd19* expression and/or function were altered in B cells from VAV-CKO mice. While the *Cd19* transcript and protein levels were normal in FO and MZ B cells from VAV-CKO mice, the levels of CD19 phosphorylation in these cells were substantially higher than those in control cells, both before and after stimulation with anti-IgM (Fig. 5B, C). Phosphorylation of Akt and PLCγ, two downstream components of the CD19 signaling pathway [46, 47], was also elevated in B cells from VAV-CKO mice in response to anti-IgM stimulation, whereas phosphorylation of the BCR component CD79a was not altered (Fig. S5E). Compared to WT B cells, B cells from CD19-CKO mice showed a 50% reduction in CD19 expression (as expected) but similar levels of CD19 phosphorylation after stimulation with anti-IgM (Fig. 5D, Fig. S5F), suggesting an approximately 2-fold increase in CD19 phosphorylation in the absence of Zbtb24. Based on these results, we hypothesized that enhanced CD19 activity contributed to the phenotype of VAV-CKO mice.

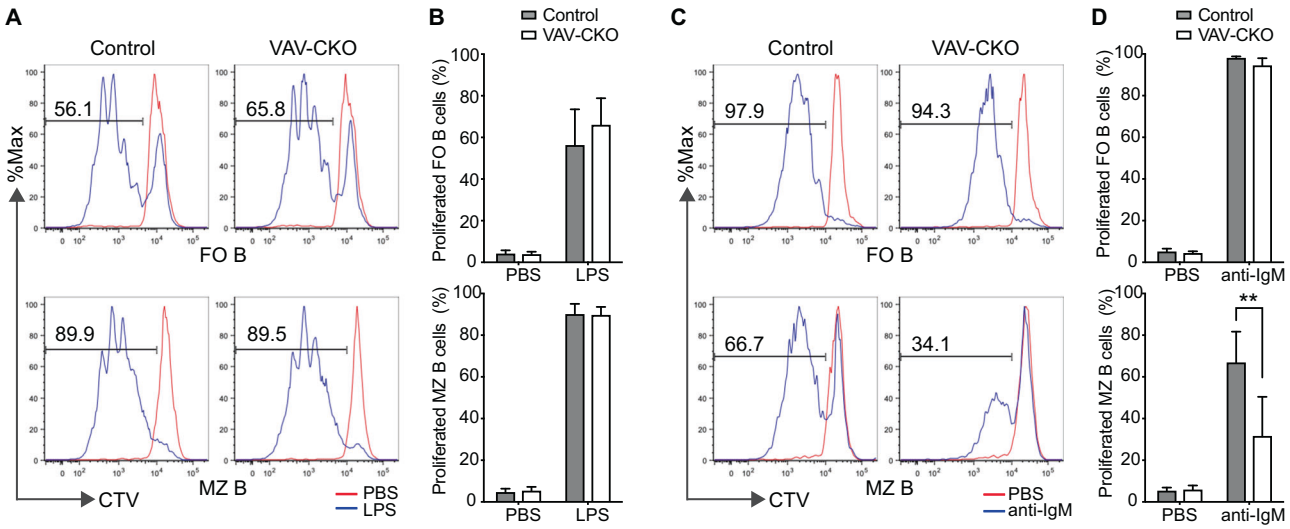

Fig. 4 *Zbtb24*-deficient MZ B-cell activation is impaired after stimulation with anti-IgM. **A**–**D** CellTrace Violet (CTV) assay showing proliferation of FO and MZ B cells from Control and VAV-CKO mice after 72 h of stimulation with LPS (**A**, **B**) or anti-IgM (**C**, **D**), with cells treated with PBS serving as unstimulated controls. Representative flow cytometry data (**A**, **C**) and percentages (mean ± SD from 8 mice per genotype) of proliferated FO and MZ B cells (**B**, **D**) are shown. Statistical analysis was performed using t test with the Mann–Whitney test. $^{**}P < 0.01$

To test this hypothesis, we generated VAV-CKO mice that were heterozygous for *Cd19* by introducing the CD19-Cre KI allele through breeding. In contrast to hypogammaglobulinemia in VAV-CKO mice (Fig. 1), *VavCre:Cd19Cre:Zbtb24*$^{2lox/2lox}$ (VAV/CD19-CKO) mice had normal levels of serum IgG1, IgM and IgA (Fig. 5A). Similarly, B cells from VAV/CD19-CKO mice no longer exhibited hyperphosphorylation of CD19 in response to stimulation with anti-IgM (Fig. 5E). VAV/CD19-CKO mice, as well as CD19-CKO mice, also showed normal humoral immune responses to immunization with NP-KLH (Fig. 5F) and NP-Ficoll (Fig. 5G). Consistent with the in vivo data, sorted FO and MZ B cells from VAV/CD19-CKO and CD19-CKO mice proliferated normally after stimulation with anti-IgM, unlike MZ B cells from VAV-CKO mice, which were defective in proliferation (Fig. 5H). Taken together, these results demonstrate that the immune phenotype of VAV-CKO mice can be rescued by reducing *Cd19* expression, thus supporting our hypothesis. Our results can also explain the apparent lack of an immune phenotype in CD19-CKO mice. While analysis of VAV-CKO mice suggests that hypogammaglobulinemia associated with *Zbtb24* deficiency is mainly caused by B-cell defects, deleting *Zbtb24* with a B-cell-specific Cre other than CD19 KI Cre would further validate this notion.

Il5ra derepression, due to loss of promoter methylation, contributes to enhanced CD19 activity in *Zbtb24*-deficient B cells

To explore the molecular mechanism by which *Zbtb24* deficiency leads to enhanced CD19 phosphorylation, we performed RNA-Seq using sorted naïve FO and MZ B cells from control and VAV-CKO mice. Bioinformatics analysis, using adjusted p value < 0.05 as the significance cutoff, identified only small numbers of differentially expressed genes in *Zbtb24*-deficient samples—43 genes (21 downregulated and 22 upregulated) in FO B cells and 35 genes (11 downregulated and 24 upregulated) in MZ B cells—with 24 common genes (8 downregulated and 16 upregulated) in both FO and MZ B cells (Fig. 6A). Some of the common downregulated genes, including *Cdca7*, *Taf6*, *Cdc40*, and *Ostc*, have been identified as direct target genes of Zbtb24 in other cell types [16, 17]. Interestingly, among the common upregulated genes were *Crisp3* (cysteine-rich secretory protein 3) and *Il5ra*, which have been implicated in B-cell functions [48–51]. RT-qPCR analysis verified the downregulation of *Cdca7* and upregulation of *Crisp3* and *Il5ra* in *Zbtb24*-deficient FO and MZ B cells (Fig. 6B).

In an attempt to find an appropriate cell line for validation experiments, we used CRISPR/Cas9 gene editing to disrupt *Zbtb24* in CH12F3 cells, a murine B-cell lymphoma cell line that shows abundant expression of Zbtb24 and can be activated by anti-IgM [19, 52]. Multiple clones with frameshift indels on both copies of *Zbtb24* were obtained (Fig. S6A, B). *Zbtb24* ablation in CH12F3 cells resulted in gene expression changes that were similar to those in *Zbtb24*-deficient naïve B cells, including downregulation of *Cdca7* and upregulation of *Crisp3* and *Il5ra* (Fig. 6C). *Zbtb24*$^{-/-}$ CH12F3 cells also showed marked increases in CD19 phosphorylation after stimulation with anti-IgM compared to WT and *Zbtb24*$^{+/-}$ (heterozygous) CH12F3 cells (Fig. 6D).

We then investigated the relevance of *Crisp3* and *Il5ra* upregulation in enhancing CD19 phosphorylation using CH12F3 cells. While overexpression of HA-tagged Crisp3 showed no obvious effect on CD19 phosphorylation, overexpression of HA-IL-5Rα recapitulated the effect of *Zbtb24* deficiency, i.e., enhanced CD19 phosphorylation after stimulation with anti-IgM (Fig. 6E). Conversely, shRNA-mediated *Il5ra* KD in *Zbtb24*$^{-/-}$ CH12F3 cells substantially prevented the hyperphosphorylation of CD19 in response to anti-IgM stimulation (Fig. 6F, G).

Il5ra encodes the IL-5-binding subunit of the IL-5 receptor. We, therefore, assessed the possibility that increased IL-5 signaling contributes to enhanced CD19 phosphorylation in *Zbtb24*-deficient B cells. Indeed, IL-5 treatment (10 ng/ml for 5 min) induced markedly higher CD19 phosphorylation in *Zbtb24*$^{-/-}$ CH12F3 cells than in WT CH12F3 cells (Fig. 6H). However, cytometric bead assay revealed that the serum IL-5 level was normal in VAV-CKO mice compared to that in WT mice (Fig. 6I) and the value reported previously [53]. It remains to be determined whether the effect of IL-5Rα on CD19 phosphorylation in vivo is dependent on IL-5.

Zbtb24 generally acts as a transcriptional activator, with *Cdca7* being a major downstream target that mediates the effect of Zbtb24 on DNA methylation [16, 17]. Given that *Il5ra* was upregulated in *Zbtb24*-deficient cells, it is unlikely that Zbtb24 directly regulates *Il5ra* transcription. Thus, we assessed the methylation status of a GC-rich region in the *Il5ra* promoter. Bisulfite sequencing analysis revealed that the region, which contains seven CpG dinucleotides, is highly methylated in WT B

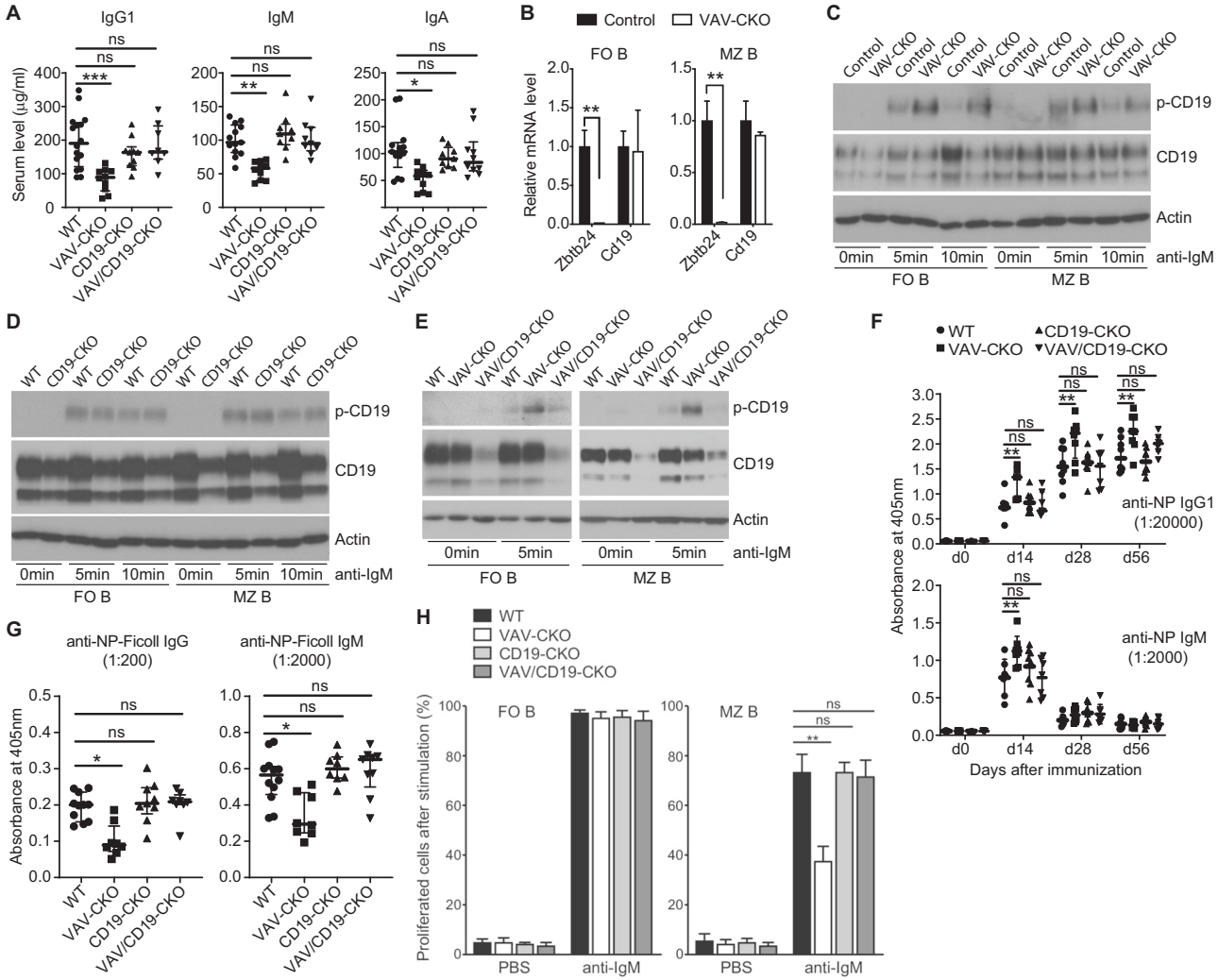

Fig. 5 The immune phenotype of VAV-CKO mice is largely due to enhanced CD19 phosphorylation. **A** Basal IgG1, IgM and IgA levels (median with interquartile range) in sera from 8- to 10-week-old WT, VAV-CKO, CD19-CKO (*Cd19Cre:Zbtb24*$^{2lox/2lox}$), and VAV/CD19-CKO (*VavCre:Cd19Cre:Zbtb24*$^{2lox/2lox}$) mice. **B** RT–qPCR data (mean+SD from 3 mice per genotype) showing relative mRNA levels of *Zbtb24* and *Cd19* in sorted FO and MZ B cells from Control and VAV-CKO mice. **C**–**E** Western blots showing the levels of phosphorylated CD19 (p-CD19) and total CD19 in sorted FO and MZ B cells from control and VAV-CKO mice (**C**), WT and CD19-CKO mice (**D**) or WT, VAV-CKO and VAV/CD19-CKO mice (**E**) that were unstimulated (0 min) or stimulated with anti-IgM for 5 or 10 min. **F** Anti-NP-specific IgG1 and IgM antibody absorbance by ELISA (median with interquartile range) in sera from WT, VAV-CKO, CD19-CKO, and VAV/CD19-CKO mice on day 0, day 14, day 28, and day 56 after immunization with NP-KLH. **G** Anti-NP-specific IgG and IgM antibody absorbance by ELISA (median with interquartile range) in sera from WT, VAV-CKO, CD19-CKO, and VAV/CD19-CKO mice on day 6 after immunization with NP-Ficoll. **H** Percentages of proliferated FO and MZ B cells from WT, VAV-CKO, CD19-CKO, and VAV/CD19-CKO mice after 72 h of stimulation with PBS or anti-IgM by CTV assay. Statistical analysis was performed using one-way ANOVA for multiple comparisons vs. WT (**A**, **G**, **H**), two-way ANOVA for multiple comparisons vs. WT (**F**), or t test with the Mann–Whitney test (**B**). **P* < 0.05; ***P* < 0.01; ****P* < 0.001; ns, not significant

cells but almost completely unmethylated in *Zbtb24*-deficient B cells (Fig. 6J). Collectively, these results indicate that the Zbtb24-Cdca7 axis represses *Il5ra* in B cells by inducing promoter methylation and that, in the absence of Zbtb24, *Il5a* derepression contributes to enhanced CD19 activity.

DISCUSSION

ICF syndrome was first reported in the 1970s [54–56]. However, little progress has been made in understanding the pathogenesis of the life-threatening hypogammaglobulinemia phenotype, partly because of the lack of appropriate animal models. Modeling ICF syndrome in mice has been discouraging. Complete inactivation of *Dnmt3b* leads to embryonic lethality [8]. Although mice carrying ICF-like *Dnmt3b* missense mutations are viable and exhibit some features of ICF syndrome, such as hypomethylation of satellite DNA and cranial facial abnormalities, they do not exhibit antibody deficiency [57]. Recent work suggests that Zbtb24 and Hells are involved in class-switching recombination (CSR) [58, 59]. However, the significance of CSR impairment in immunodeficiency in ICF syndrome remains to be determined. B cells from ICF patients have been shown to be competent for CSR in vitro [20]. Many ICF patients show deficiency in IgM, among other Ig isotypes, which cannot be explained by defective CSR. In this study, we show that mice deficient in *Zbtb24* in the hematopoietic lineage (VAV-CKO mice) recapitulate major clinical features of ICF syndrome, including decreased levels of IgM, IgG1, and IgA, thus providing a valuable mouse model of this rare human disease.

Similar to ICF patients, who usually have normal T- and B-cell counts but lack plasma cells [1, 2, 20], VAV-CKO mice exhibit no abnormalities in lymphocyte development but display decreases

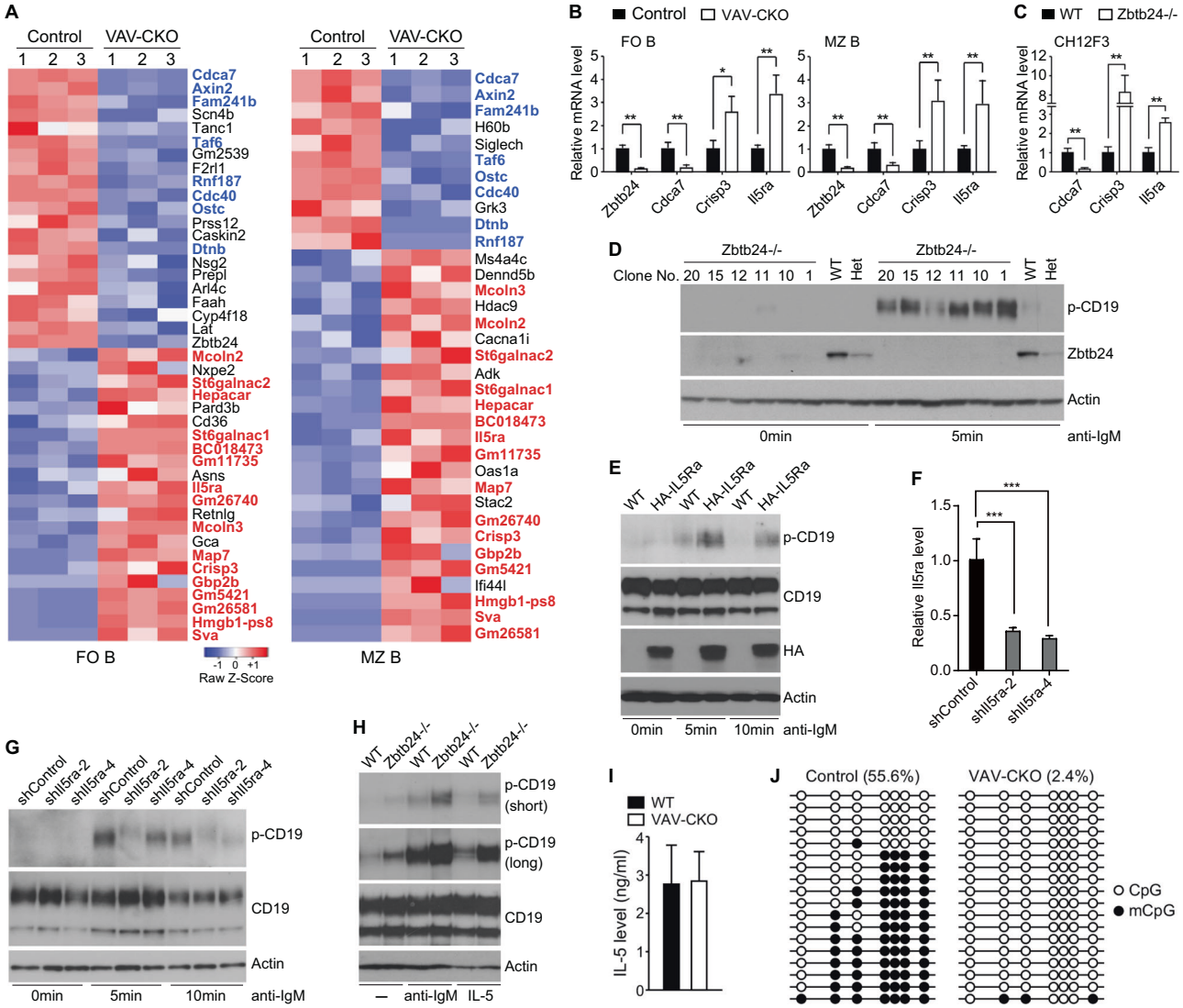

Fig. 6 *Il5ra* derepression associated with promoter hypomethylation contributes to increased CD19 phosphorylation in *Zbtb24*-deficient B cells. **A** Heatmap of differentially expressed genes in naïve FO and MZ B cells from Control and VAV-CKO mice identified by RNA-Seq. Genes that are downregulated and upregulated in both FO and MZ B cells are highlighted in blue and red, respectively. **B**, **C** RT–qPCR analysis verifying downregulation of *Cdca7* and upregulation of *Crisp3* and *Il5ra* in *Zbtb24*-deficient FO and MZ B cells (**B**) and in *Zbtb24*$^{-/-}$ CH12F3 cells (**C**). **D** Western blots showing that after stimulation with IgM, CD19 phosphorylation is dramatically enhanced in *Zbtb24*$^{-/-}$ CH12F3 cells compared to WT and *Zbtb24*$^{+/-}$ (Het) CH12F3 cells. **E** Overexpression of HA-tagged IL-5Rα in CH12F3 cells recapitulates the effect of *Zbtb24* deficiency on CD19 phosphorylation. **F**, **G** shRNA-mediated *Il5ra* knockdown in *Zbtb24*$^{-/-}$ CH12F3 cells reduces CD19 phosphorylation in response to anti-IgM stimulation. Shown are RT–qPCR data demonstrating the knockdown effects of the two most efficient *Il5ra* shRNAs, i.e., *shIl5ra-2* and *shIl5ra-4* (**F**) and Western blots with the indicated antibodies (**G**). **H** Western blots showing that IL-5 treatment (10 ng/ml for 5 min) induces enhanced CD19 phosphorylation in *Zbtb24*$^{-/-}$ CH12F3 cells, similar to the effect of anti-IgM. **I** IL-5 levels in serum samples from WT and VAV-CKO mice (mean + SD from three mice per genotype), which show no difference. **J** Bisulfite sequencing analysis of a GC-rich region (containing seven CpG dinucleotides) in the *Il5ra* promoter, which shows hypermethylation in WT B cells but almost complete loss of methylation in *Zbtb24*-deficient B cells. Statistical analysis was performed using t test with the Mann Whitey test (**B**, **C**) or one-way ANOVA for multiple comparisons vs. shControl (**F**). *$P < 0.05$; **$P < 0.01$

in plasma cells, suggesting impaired B-cell activation and/or terminal differentiation. The immune defects associated with *Zbtb24* deficiency appear to be independent of T cells, as cytokine secretion by helper T cells from VAV-CKO mice is unaltered; moreover, mice with *Zbtb24* deleted in T cells (by Lck-Cre) exhibit no obvious immune phenotype. Therefore, our work focused on B cells. We show that MZ B cells from VAV-CKO mice are severely defective in proliferation after in vitro stimulation with the soluble F(ab')2 fragments of anti-IgM, while their response to LPS stimulation is unaffected. Consistent with the in vitro results, immunization experiments revealed that VAV-CKO mice are hyporesponsive to the TI-2 antigens NP-Ficoll and NP-dextran but exhibit a normal response to the TI-1 antigen NP-LPS. Antigen-activated MZ B cells rapidly differentiate into plasma cells that secrete antibodies (primarily IgM) that provide innate-like immunity against blood-borne pathogens [60]. Our results indicate that activation of *Zbtb24*-deficient MZ B cells by TI-2 antigens is defective, which likely contributes to IgM deficiency in VAV-CKO mice. The decreased levels of other isotypes (e.g., IgG1 and IgA) in these mice could be secondary to IgM deficiency and/or due to CSR impairment [59].

In contrast to diminished TI-2 responses, VAV-CKO mice are hyperresponsive to immunization with the TD antigen NP-KLH. Interestingly, B-cell-specific deletion of *Dnmt3a* and *Dnmt3b* in

mice results in a similar phenotype: normal B-cell development and enhanced TD responses upon immunization [45]. Notably, B cells from ICF patients have also been shown to respond more robustly to BCR stimulation than those from healthy donors [20]. Taken together, these observations indicate that abnormally enhanced TD responses, mediated mainly by FO B cells, may also contribute to immunodeficiency in ICF syndrome. Our data show that VAV-CKO mice tend to produce low-affinity antibodies in response to immunization, thus suggesting the possible involvement of Zbtb24 in antibody affinity maturation.

The divergent responses of VAV-CKO mice to different antigens, i.e., enhanced TD and diminished TI-2 responses, are reminiscent of the phenotype of hCD19TG mice [27]. CD19 functions as a thresholding controller of BCR signaling in response to TD and TI antigens, whereby the loss of CD19 inhibits TD and TI-1 antigen responses in mice, while overexpressing hCD19 in mice inhibits the TI-2 antigen response. We show that although CD19 expression is not affected by *Zbtb24* deficiency, B cells from VAV-CKO mice, as well as *Zbtb24*-deficient CH12F3 cells, display substantially elevated CD19 phosphorylation, both before and after stimulation with anti-IgM. Importantly, the immune defects of VAV-CKO mice, including antibody deficiency, can be reversed by disrupting one copy of *Cd19* in these mice. These results demonstrate that Zbtb24 is a negative regulator of CD19 activity and that enhanced CD19 activation is largely responsible for immunodeficiency in VAV-CKO mice. CD19 positively modulates BCR signaling by lowering thresholds for activation and enhancing signaling events [28]. Indeed, B cells from ICF patients, relative to those from healthy individuals, are more readily activated in response to BCR stimulation in vitro [20], which may be related to enhanced CD19 activation.

RNA-Seq analysis of naïve B cells from VAV-CKO and control mice identified only dozens of differentially expressed genes, including several known Zbtb24 target genes, such as *Cdca7*, *Taf6*, *Ostc,* and *Cdc40* [16, 17], suggesting that Zbtb24 regulates the expression of a limited number of genes. By gain- and loss-of-function experiments using CH12F3 cells, we validated that upregulation of *Il5ra* contributes to enhanced CD19 activation in *Zbtb24*-deficient B cells. While IL-5Rα is constitutively expressed in and needed for the development and functions of eosinophils and B-1 cells, it is not expressed in naïve B-2 (MZ and FO B) cells [61–65]. In the absence of Zbtb24, IL-5Rα expression on B-2 cells could trigger IL-5 signaling, even though we observed no changes in serum IL-5 levels in VAV-CKO mice. Previous work suggests that IL-5 signaling augments plasma cell differentiation by enhancing *Blimp1* expression [66], consistent with our finding that VAV-CKO mice show an enhanced TD humoral immune response. It would be interesting to determine whether CD19 activity and *Blimp1* expression are linked. Also worth noting is that we cannot exclude the possibility that enhanced CD19 activity and other immune defects observed in VAV-CKO mice are related to noncanonical effects of IL-5Rα independent of the ligand (IL-5). Considering that CD19 activation has distinct effects on different subtypes of B cells, hypogammaglobulinemia associated with *Zbtb24* deficiency is perhaps mainly due to reduced production of natural antibodies because of diminished humoral immune responses to TI-2 antigens by MZ B cells (Fig. S7).

Loss of DNA methylation in specific genomic regions is believed to be the primary defect in ICF syndrome. In contrast to the well-documented hypomethylation of classical satellite repeats in centromeric and pericentromeric regions [6], little is known about the genes affected by DNA methylation that are relevant to the pathogenesis of ICF syndrome. We identified a GC-rich region in the *Il5ra* promoter as hypermethylated in normal naïve B cells but almost completely unmethylated in *Zbtb24*-deficient B cells. Our results suggest that the Zbtb24-Cdca7 axis, by inducing or maintaining promoter methylation, is a critical component of the mechanism needed to keep *Il5ra* repressed in resting B cells. Although the sequences of the human and mouse *Il5ra* promoter regions are not highly conserved, both contain GC-rich regions, and CpG methylation may profoundly affect binding by transcription factors and other important regulators.

In summary, we show that mice deficient in *Zbtb24* in the hematopoietic lineage recapitulate the hypogammaglobulinemia phenotype of ICF patients. Characterization of this animal model revealed that *Zbtb24* deficiency in B cells results in loss of DNA methylation in the *Il5ra* promoter region, and derepression of *Il5a* leads to enhanced CD19 phosphorylation, thus contributing to immunodeficiency (Fig. S7). Therapeutics targeting IL-5, IL-5Rα, CD19, and BCR signaling have been developed for various diseases [67–69]. Our findings suggest the possibility of using some of these therapeutics to treat patients with ICF syndrome.

REFERENCES

1. Hagleitner MM, Lankester A, Maraschio P, Hulten M, Fryns JP, Schuetz C, et al. Clinical spectrum of immunodeficiency, centromeric instability and facial dysmorphism (ICF syndrome). J Med Genet. 2008;45:93–9.
2. Weemaes CM, van Tol MJ, Wang J, van Ostaijen-ten Dam MM, van Eggermond MC, Thijssen PE, et al. Heterogeneous clinical presentation in ICF syndrome: correlation with underlying gene defects. Eur J Hum Genet. 2013;21:1219–25.
3. Maraschio P, Zuffardi O, Dalla Fior T, Tiepolo L. Immunodeficiency, centromeric heterochromatin instability of chromosomes 1, 9, and 16, and facial anomalies: the ICF syndrome. J Med Genet. 1988;25:173–80.
4. Jeanpierre M, Turleau C, Aurias A, Prieur M, Ledeist F, Fischer A, et al. An embryonic-like methylation pattern of classical satellite DNA is observed in ICF syndrome. Hum Mol Genet. 1993;2:731–5.
5. Tuck-Muller CM, Narayan A, Tsien F, Smeets DF, Sawyer J, Fiala ES, et al. DNA hypomethylation and unusual chromosome instability in cell lines from ICF syndrome patients. Cytogenet Cell Genet. 2000;89:121–8.
6. Velasco G, Grillo G, Touleimat N, Ferry L, Ivkovic I, Ribierre F, et al. Comparative methylome analysis of ICF patients identifies heterochromatin loci that require ZBTB24, CDCA7 and HELLS for their methylated state. Hum Mol Genet. 2018;27:2409–24.
7. Xu GL, Bestor TH, Bourc'his D, Hsieh CL, Tommerup N, Bugge M, et al. Chromosome instability and immunodeficiency syndrome caused by mutations in a DNA methyltransferase gene. Nature. 1999;402:187–91.
8. Okano M, Bell DW, Haber DA, Li E. DNA methyltransferases Dnmt3a and Dnmt3b are essential for de novo methylation and mammalian development. Cell. 1999;99:247–57.
9. Hansen RS, Wijmenga C, Luo P, Stanek AM, Canfield TK, Weemaes CM, et al. The DNMT3B DNA methyltransferase gene is mutated in the ICF immunodeficiency syndrome. Proc Natl Acad Sci USA. 1999;96:14412–7.
10. de Greef JC, Wang J, Balog J, den Dunnen JT, Frants RR, Straasheijm KR, et al. Mutations in ZBTB24 are associated with immunodeficiency, centromeric instability, and facial anomalies syndrome type 2. Am J Hum Genet. 2011;88:796–804.
11. Chouery E, Abou-Ghoch J, Corbani S, El Ali N, Korban R, Salem N, et al. A novel deletion in ZBTB24 in a Lebanese family with immunodeficiency, centromeric instability, and facial anomalies syndrome type 2. Clin Genet. 2012;82:489–93.
12. Nitta H, Unoki M, Ichiyanagi K, Kosho T, Shigemura T, Takahashi H, et al. Three novel ZBTB24 mutations identified in Japanese and Cape Verdean type 2 ICF syndrome patients. J Hum Genet. 2013;58:455–60.
13. Thijssen PE, Ito Y, Grillo G, Wang J, Velasco G, Nitta H, et al. Mutations in CDCA7 and HELLS cause immunodeficiency-centromeric instability-facial anomalies syndrome. Nat Commun. 2015;6:7870.
14. Wu H, Thijssen PE, de Klerk E, Vonk KK, Wang J, den Hamer B, et al. Converging disease genes in ICF syndrome: ZBTB24 controls expression of CDCA7 in mammals. Hum Mol Genet. 2016;25:4041–51.
15. Jenness C, Giunta S, Muller MM, Kimura H, Muir TW, Funabiki H. HELLS and CDCA7 comprise a bipartite nucleosome remodeling complex defective in ICF syndrome. Proc Natl Acad Sci USA. 2018;115:E876–E85.
16. Thompson JJ, Kaur R, Sosa CP, Lee JH, Kashiwagi K, Zhou D, et al. ZBTB24 is a transcriptional regulator that coordinates with DNMT3B to control DNA methylation. Nucleic Acids Res. 2018;46:10034–51.
17. Ren R, Hardikar S, Horton JR, Lu Y, Zeng Y, Singh AK, et al. Structural basis of specific DNA binding by the transcription factor ZBTB24. Nucleic Acids Res. 2019;47:8388–98.
18. Unoki M, Funabiki H, Velasco G, Francastel C, Sasaki H. CDCA7 and HELLS mutations undermine nonhomologous end joining in centromeric instability syndrome. J Clin Investig. 2019;129:78–92.

19. Hardikar S, Ying Z, Zeng Y, Zhao H, Liu B, Veland N, et al. The ZBTB24-CDCA7 axis regulates HELLS enrichment at centromeric satellite repeats to facilitate DNA methylation. Protein Cell. 2020;11:214–8.
20. Blanco-Betancourt CE, Moncla A, Milili M, Jiang YL, Viegas-Pequignot EM, Roquelaure B, et al. Defective B-cell-negative selection and terminal differentiation in the ICF syndrome. Blood. 2004;103:2683–90.
21. Kraus M, Alimzhanov MB, Rajewsky N, Rajewsky K. Survival of resting mature B lymphocytes depends on BCR signaling via the Igalpha/beta heterodimer. Cell. 2004;117:787–800.
22. Victora GD, Nussenzweig MC. Germinal centers. Annu Rev Immunol. 2022;40:413–42.
23. Meffre E. The establishment of early B cell tolerance in humans: lessons from primary immunodeficiency diseases. Ann NY Acad Sci. 2011;1246:1–10.
24. Engel P, Zhou LJ, Ord DC, Sato S, Koller B, Tedder TF. Abnormal B lymphocyte development, activation, and differentiation in mice that lack or overexpress the CD19 signal transduction molecule. Immunity. 1995;3:39–50.
25. Rickert RC, Rajewsky K, Roes J. Impairment of T-cell-dependent B-cell responses and B-1 cell development in CD19-deficient mice. Nature. 1995;376:352–5.
26. Zhou LJ, Smith HM, Waldschmidt TJ, Schwarting R, Daley J, Tedder TF. Tissue-specific expression of the human CD19 gene in transgenic mice inhibits antigen-independent B-lymphocyte development. Mol Cell Biol. 1994;14:3884–94.
27. Sato S, Steeber DA, Tedder TF. The CD19 signal transduction molecule is a response regulator of B-lymphocyte differentiation. Proc Natl Acad Sci USA. 1995;92:11558–62.
28. Tedder TF. CD19: a promising B cell target for rheumatoid arthritis. Nat Rev Rheumatol. 2009;5:572–7.
29. Farley FW, Soriano P, Steffen LS, Dymecki SM. Widespread recombinase expression using FLPeR (flipper) mice. Genesis. 2000;28:106–10.
30. Lewandoski M, Wassarman KM, Martin GR. Zp3-cre, a transgenic mouse line for the activation or inactivation of loxP-flanked target genes specifically in the female germ line. Curr Biol. 1997;7:148–51.
31. Georgiades P, Ogilvy S, Duval H, Licence DR, Charnock-Jones DS, Smith SK, et al. VavCre transgenic mice: a tool for mutagenesis in hematopoietic and endothelial lineages. Genesis. 2002;34:251–6.
32. Wang Q, Strong J, Killeen N. Homeostatic competition among T cells revealed by conditional inactivation of the mouse Cd4 gene. J Exp Med. 2001;194:1721–30.
33. Rickert RC, Roes J, Rajewsky K. B lymphocyte-specific, Cre-mediated mutagenesis in mice. Nucleic Acids Res. 1997;25:1317–8.
34. Ying Z, Mei M, Zhang P, Liu C, He H, Gao F, et al. Histone arginine methylation by PRMT7 controls germinal center formation via regulating Bcl6 transcription. J Immunol. 2015;195:1538–47.
35. Kim D, Pertea G, Trapnell C, Pimentel H, Kelley R, Salzberg SL. TopHat2: accurate alignment of transcriptomes in the presence of insertions, deletions and gene fusions. Genome Biol. 2013;14:R36.
36. Langmead B, Salzberg SL. Fast gapped-read alignment with Bowtie 2. Nat Methods. 2012;9:357–9.
37. Anders S, Pyl PT, Huber W. HTSeq-a Python framework to work with high-throughput sequencing data. Bioinformatics. 2015;31:166–9.
38. Love MI, Huber W, Anders S. Moderated estimation of fold change and dispersion for RNA-seq data with DESeq2. Genome Biol. 2014;15:550.
39. Veland N, Lu Y, Hardikar S, Gaddis S, Zeng Y, Liu B, et al. DNMT3L facilitates DNA methylation partly by maintaining DNMT3A stability in mouse embryonic stem cells. Nucleic Acids Res. 2019;47:152–67.
40. Zeng Y, Ren R, Kaur G, Hardikar S, Ying Z, Babcock L, et al. The inactive Dnmt3b3 isoform preferentially enhances Dnmt3b-mediated DNA methylation. Genes Dev. 2020;34:1546–58.
41. Cerbone M, Wang J, Van der Maarel SM, D'Amico A, D'Agostino A, Romano A, et al. Immunodeficiency, centromeric instability, facial anomalies (ICF) syndrome, due to ZBTB24 mutations, presenting with large cerebral cyst. Am J Med Genet A. 2012;158A:2043–6.
42. Kiaee F, Zaki-Dizaji M, Hafezi N, Almasi-Hashiani A, Hamedifar H, Sabzevari A, et al. Clinical, Immunologic and molecular spectrum of patients with immunodeficiency, centromeric instability, and facial anomalies (ICF) syndrome: a systematic review. Endocr Metab Immune Disord Drug Targets. 2021;21:664–72.
43. Sterlin D, Velasco G, Moshous D, Touzot F, Mahlaoui N, Fischer A, et al. Genetic, cellular and clinical features of ICF syndrome: a French national survey. J Clin Immunol. 2016;36:149–59.
44. Kamae C, Imai K, Kato T, Okano T, Honma K, Nakagawa N, et al. Clinical and Immunological Characterization of ICF Syndrome in Japan. J Clin Immunol. 2018;38:927–37.
45. Barwick BG, Scharer CD, Martinez RJ, Price MJ, Wein AN, Haines RR, et al. B cell activation and plasma cell differentiation are inhibited by de novo DNA methylation. Nat Commun. 2018;9:1900.
46. Hendriks RW, Yuvaraj S, Kil LP. Targeting Bruton's tyrosine kinase in B cell malignancies. Nat Rev Cancer. 2014;14:219–32.
47. Ortiz-Maldonado V, Garcia-Morillo M, Delgado J. The biology behind PI3K inhibition in chronic lymphocytic leukaemia. Ther Adv Hematol. 2015;6:25–36.
48. Pfisterer P, Konig H, Hess J, Lipowsky G, Haendler B, Schleuning WD, et al. CRISP-3, a protein with homology to plant defense proteins, is expressed in mouse B cells under the control of Oct2. Mol Cell Biol. 1996;16:6160–8.
49. Sato S, Katagiri T, Takaki S, Kikuchi Y, Hitoshi Y, Yonehara S, et al. IL-5 receptor-mediated tyrosine phosphorylation of SH2/SH3-containing proteins and activation of Bruton's tyrosine and Janus 2 kinases. J Exp Med. 1994;180:2101–11.
50. Koike M, Kikuchi Y, Tominaga A, Takaki S, Akagi K, Miyazaki J, et al. Defective IL-5-receptor-mediated signaling in B cells of X-linked immunodeficient mice. Int Immunol. 1995;7:21–30.
51. Horikawa K, Takatsu K. Interleukin-5 regulates genes involved in B-cell terminal maturation. Immunology. 2006;118:497–508.
52. Whillock AL, Ybarra TK, Bishop GA. TNF receptor-associated factor 3 restrains B-cell receptor signaling in normal and malignant B cells. J Biol Chem. 2021;296:100465.
53. Litman PM, Day A, Kelley TJ, Darrah RJ. Serum inflammatory profiles in cystic fibrosis mice with and without Bordetella pseudohinzii infection. Sci Rep. 2021;11:17535.
54. Hulten M. Selective somatic pairing and fragility at 1q12 in a boy with common variable immuno deficiency. Clin Genet. 1978;14:294.
55. Tiepolo L, Maraschio P, Gimelli G, Cuoco C, Gargani GF, Romano C. Concurrent instability at specific sites of chromosomes 1, 9 and 16 resulting in multibranched structures. Clin Genet. 1978;14:313–4.
56. Tiepolo L, Maraschio P, Gimelli G, Cuoco C, Gargani GF, Romano C. Multibranched chromosomes 1, 9, and 16 in a patient with combined IgA and IgE deficiency. Hum Genet. 1979;51:127–37.
57. Ueda Y, Okano M, Williams C, Chen T, Georgopoulos K, Li E. Roles for Dnmt3b in mammalian development: a mouse model for the ICF syndrome. Development. 2006;133:1183–92.
58. He Y, Ren J, Xu X, Ni K, Schwader A, Finney R, et al. Lsh/HELLS is required for B lymphocyte development and immunoglobulin class switch recombination. Proc Natl Acad Sci USA. 2020;117:20100–8.
59. Helfricht A, Thijssen PE, Rother MB, Shah RG, Du L, Takada S, et al. Loss of ZBTB24 impairs nonhomologous end-joining and class-switch recombination in patients with ICF syndrome. J Exp Med. 2020;217:e20191688.
60. Cerutti A, Cols M, Puga I. Marginal zone B cells: virtues of innate-like antibody-producing lymphocytes. Nat Rev Immunol. 2013;13:118–32.
61. Hitoshi Y, Yamaguchi N, Mita S, Sonoda E, Takaki S, Tominaga A, et al. Distribution of IL-5 receptor-positive B cells. Expression of IL-5 receptor on Ly-1(CD5)+ B cells. J Immunol. 1990;144:4218–25.
62. Kopf M, Brombacher F, Hodgkin PD, Ramsay AJ, Milbourne EA, Dai WJ, et al. IL-5-deficient mice have a developmental defect in CD5+ B-1 cells and lack eosinophilia but have normal antibody and cytotoxic T cell responses. Immunity. 1996;4:15–24.
63. Moon BG, Takaki S, Miyake K, Takatsu K. The role of IL-5 for mature B-1 cells in homeostatic proliferation, cell survival, and Ig production. J Immunol. 2004;172:6020–9.
64. Takatsu K, Nakajima H. IL-5 and eosinophilia. Curr Opin Immunol. 2008;20:288–94.
65. Yoshida T, Ikuta K, Sugaya H, Maki K, Takagi M, Kanazawa H, et al. Defective B-1 cell development and impaired immunity against Angiostrongylus cantonensis in IL-5R alpha-deficient mice. Immunity. 1996;4:483–94.
66. Emslie D, D'Costa K, Hasbold J, Metcalf D, Takatsu K, Hodgkin PO, et al. Oct2 enhances antibody-secreting cell differentiation through regulation of IL-5 receptor alpha chain expression on activated B cells. J Exp Med. 2008;205:409–21.
67. Anagnostou T, Riaz IB, Hashmi SK, Murad MH, Kenderian SS. Anti-CD19 chimeric antigen receptor T-cell therapy in acute lymphocytic leukaemia: a systematic review and meta-analysis. Lancet Haematol. 2020;7:e816–e26.
68. Burger JA, Wiestner A. Targeting B cell receptor signalling in cancer: preclinical and clinical advances. Nat Rev Cancer. 2018;18:148–67.
69. Principe S, Porsbjerg C, Bolm Ditlev S, Kjaersgaard Klein D, Golebski K, Dyhre-Petersen N, et al. Treating severe asthma: Targeting the IL-5 pathway. Clin Exp Allergy. 2021;51:992–1005.

ACKNOWLEDGEMENTS

We thank Drs. Margarida Albuquerque Almeida Santos and Momoko Yoshimoto-Kobayashi for discussions and Ms. Zaowen Chen for technical assistance. The work was supported by grants (1R01AI12140301A1 to TC; CA16672 to CCSG Cores at MD Anderson Cancer Center) from National Institutes of Health (NIH), Core Facility Support Award (RP170002 to JS) from Cancer Prevention and Research Institute of Texas (CPRIT), and next-generation sequencing (NGS) allowances from the Center for Cancer Epigenetics (CCE) at MD Anderson Cancer Center. ZY received a fellowship from the Sam and Freda Davis Fund. TH received a CCE Scholarship.

AUTHOR CONTRIBUTIONS

ZY, KMM, and TC designed the research and wrote the manuscript; ZY, SH, JBP, TH, and YM performed the experiments; YC and JS performed the RNA-Seq; BL performed the bioinformatics analysis; ZY, YM, KMM, and TC analyzed the data.

FUNDING

This study was supported by a grant (1R01AI12140301A1) from the National Institutes of Health (NIH) in the USA.

COMPETING INTERESTS

The authors declare no competing interests.

ADDITIONAL INFORMATION

Supplementary information The online version contains supplementary material available at https://doi.org/10.1038/s41423-023-01106-w.

Correspondence and requests for materials should be addressed to Kevin M. McBride or Taiping Chen.